Eco-Friendly Synthesis of Titanium Dioxide Doped Tin-Zirconium Oxide Nanocomposites for the Degradation of Brilliant Green and 4-Nitrophenol

Sirajul Haq[1*], Umarah Mushtaq[2], Sadiq Ur Rehman[2], Manel Ben Ali[3], Shafia Shujaat[2], Jamoliddin Razzokov[1,4,5], Raja Amjad Waheed Khan[2], Fehmi Boufahja[6], Ezzeddine Mahmoudi[7], Amor Hedfi[3]

[1] Institute of Fundamental and Applied Research, National Research University TIIAME, Kori Niyoziy 39, Tashkent 100000, Uzbekistan

[2] Department of Chemistry, University of Azad Jammu and Kashmir, Muzaffarabad 13100, Pakistan.

[3] Department of Biology, College of Sciences, Taif University, PO Box 11099, Taif 21944, Saudi Arabia.

[4] *Department of Microbiology, Pharmacology, Normal and Pathological Physiology, Kokand University Andijan Branch, Jasorat 43, 170619 Andijan, Uzbekistan.*

[5] Department of Biotechnology, Tashkent State Technical University, Universitet 2, Tashkent 100095, Uzbekistan.

[6] Biology Department, College of Science, Imam Mohammad Ibn Saud Islamic University (IMSIU), Riyadh, 11623, Saudi Arabia.

[7] University of Carthage, Faculty of Sciences of Bizerte, LR01ES14 Laboratory of Environment Biomonitoring, Coastal Ecology and Ecotoxicology Unit, 7021, Zarzouna, Tunisia.

* Corresponding author: cii_raj@yahoo.com

ACCEPTED MANUSCRIPT

Abstract: In this study, a green, cost-effective, and reliable method was employed to synthesize pure and titanium dioxide-doped Tin dioxide-zirconium dioxide nanocomposite (TiO_2@SnO_2-ZrO_2 NC). The synthesis strategy involves the utilization of leaf extract of the *Swertia chirayita* plant as a stabilizing and capping agent. The surface area of prepared nanocomposites was analyzed through the N_2 adsorption process, crystalline nature, and other properties of the crystal were investigated by X-ray diffraction (XRD) while scanning electron microscopy (SEM) was used to explore the morphology of pure and TiO_2@SnO_2-ZrO_2 NC. The optical properties of pure and TiO_2@SnO_2-ZrO_2 NC were determined by evaluating the band gap through diffused reflectance (DRS) spectroscopy. The functional groups were studied using Fourier Transform infrared (FTIR) spectroscopy. The photocatalytic properties of prepared pure and TiO_2@SnO_2-ZrO_2 NC were examined by performing the degradation of brilliant green and 4-nitrophenol. The incorporation of TiO_2 into SnO_2-ZrO_2 led to a decrease in the photocatalytic activity under solar light irradiation.

Graphical Abstract:

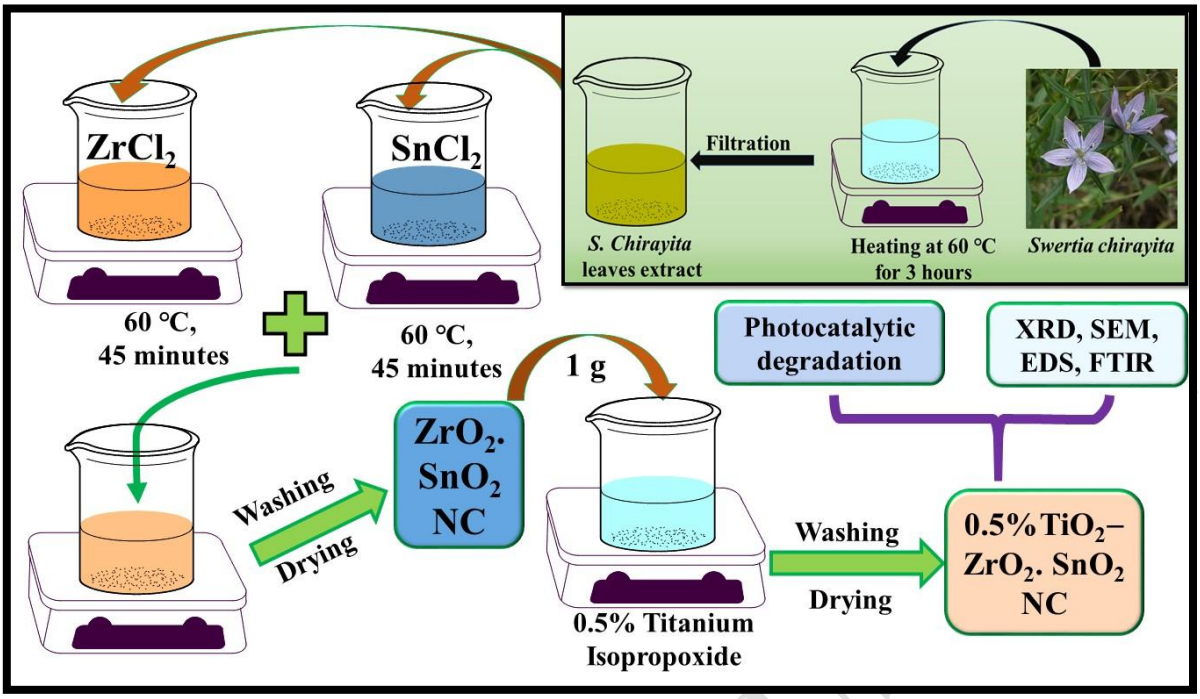

Keywords: Nanocomposite; Zirconia; Titanium; Doping; Characterization.

1 Introduction

Water is one of the most important necessities of life, covering 71% of the earth's crust. With a rapid increase in population and industrial activities, global demand for water doubles approximately every 21 years. Water quality is affected by the development and unplanned growth of the industrial sector, therefore, one of the major concerns of modern research is environmental contamination due to the Industrial Revolution (Roushan et al., 2016). The root cause of environmental pollution is industrialization which is the key factor for economic development (Malik et al., 2014). Human activities such as urbanization, farming, and industries are discharging their wastewater containing organic pollutants in freshwater reservoirs making them unfit for consumption. Improper management of waste materials, produced by different industrial sectors and other anthropogenic activities, is one of the critical issues in developing countries (State, 2011).

The textile industry is one of the major contributors to water pollution which discharges 10-25% of textile dyes in freshwater reservoirs. The annual production and usage of dyes by textile industry is 1.3 million tons (Chowdhury et al., 2019; Wibowo, Safitri, et al., 2025). Textile is a globally widespread industry, accounting for 7% of world exports, and generates 1 trillion dollars annually. The industrial sector emerges as one of the largest global polluters due to its consumption of large amounts of fuels and chemicals with 80% of effluents being discharged into water bodies (Lellis et al., 2019; Wibowo, Anwar, et al., 2025). These residual dyes not only damage the aesthetic beauty of water bodies but also affect the aquatic life. Dyes contain aromatic compounds such as naphthalene

ACCEPTED MANUSCRIPT

and benzamine which are toxic and carcinogenic. In the past, natural dyes were extracted from plants and animals; however, synthetic dyes were discovered in 1856. Complex dye families such as cationic dyes and basic dyes are used in wool, acrylic, and nylon dyeing (Konecoglu et al., 2015). Dyes are categorized into direct dyes, vat dyes, basic dyes, reactive dyes, and solvent dyes based on their chromophore structure (Anwer et al., 2019).

To treat industrial effluents that contain organic pollutants, different techniques are used. The most commonly employed technologies are adsorption, precipitation, electrochemical technologies, ion exchange membranes, and one most fruitful processes is the photodegradation of organic dyes (Wibowo et al., 2023). This process entails exposing the pollutants to UV radiation and converting them to carbon dioxide and water. The development of nanoscience and nanotechnology has captured the interest of modern researchers across various scientific fields. The photocatalytic properties of nanomaterials are enhanced owing to their distinctive characteristics like high adsorption capacity and large surface area, hence, they can be effectively used in the degradation of organic pollutants present in wastewater (Ruan et al., 2019). Over the past 2 decades, semiconductors such as ZrO_2, CeO_2, SnO_2, as well as TiO_2 have found extensive application in degrading organic pollutants, pesticides, detergents, dyes, and other volatile compounds under the influence of UV radiations (Pouretedal et al., 2012). Due to nontoxicity, high stability, and good photocatalytic activity, TiO_2 has been lavishly used for environmental decontamination. TiO_2 absorbs in the near ultraviolet region and has a band gap of 3.2 eV, rendering it unresponsive to the visible region. When either metal or non-metal elements are doped on semiconductors, their photocatalytic activity is enhanced (Sadat et al., 2016). The most promising process for wastewater treatment is photocatalysis in which semiconductors are used as photocatalysts and pollutants are degraded by generation of primary oxidant hydroxyl radical. To treat organic wastewater, SnO_2 has become a potential photocatalyst owing to its nontoxic nature, chemical stability, and low cost. Its band gap is 3.6 eV and recombination of electrons and holes occurs rapidly; however, this limitation can be mitigated by utilizing composite semiconductors and doping techniques (Haq, Rehman, et al., 2020). The photocatalytic performance of mixed metal composite, SnO_2-ZnO, is better than pure SnO_2 (Haq et al., 2022; Haq, Rehman, et al., 2021; Haq, Shoukat, et al., 2020). ZrO_2 is an n-type semiconductor whose band gap is 5.0 eV and holds excellent technological significance. It is extensively utilized in the fields of extraction, catalysis, solid electrolytes, and gas sensors because of its low toxicity and high extraction efficiency as well as adsorption capability (Haq, Afsar, Ali, et al., 2021; Haq, Afsar, Din, et al., 2021). Some other principal properties of zirconia include high hardness, good frictional behavior, high density, low thermal conductivity, temperature capability up to 2400 °C, electrical insulation, and wear resistance (Bona et al., 2015).

ACCEPTED MANUSCRIPT

Depending on the requirement and appropriateness, a variety of physical and chemical methods can be used for the synthesis of nanocomposites. Physical methods like mechanical milling, plasma, aerosol, ablation, electrodeposition, and arc discharge along with chemical methods involving hydrothermal, microemulsion, sol-gel, and sonochemical processes are commonly employed for the fabrication of nanocomposites (Karak 2019). A simple salt-assisted combustion approach was used for the synthesis of $Nd_2Sn_2O_7$-SnO_2 nanocomposite which is a highly active photocatalyst used in degrading methyl orange dye (Sadat et al., 2016). A facile hydrothermal process was employed to prepare Cerium zirconium oxide nanocomposite ($CexZryO_2$) that was used for the remediation of sulfonamide pollutants (Li et al., 2019). Thus study was planned to develop cost-effective, sustainable, and environmentally benign approaches for the synthesis of nanomaterials used in wastewater treatment. Conventional synthesis methods for photocatalysts often involve hazardous chemicals, high energy consumption, and produce toxic by-products, which limit their practical applicability, especially in developing regions. To address these challenges, our study focuses on the green fabrication of TiO_2@SnO_2-ZrO_2 NC using *S. chirayita* plant extract. The primary motivation is to utilize natural resources for the synthesis of advanced inorganic materials that are not only effective in degrading common organic pollutants like Brilliant Green and 4-Nitrophenol but also align with the principles of green chemistry. Furthermore, doping with TiO_2 is intended to enhance photocatalytic efficiency and environmental stability, broadening the scope of application in real-world wastewater remediation under solar light (Haq et al., 2018; Salama et al., 2018). *S. chirayita* is an annual, branched medicinal herb belonging to the family Gentianaceae. It grows up to 1.5 meters in height and has broad, opposite, and sessile leaves. It was initially introduced in 1839 in Edinburgh pharmacopeias to be used either as a tincture or an infusion. *S. chirayita* is a 1.5 m tall annual branching plant with broad, opposite, and sessile leaves. It is a bitter tonic that is distributed throughout temperate regions extending from Kashmir to Bhutan. It contains natural products such as terpenoids, iridoids, flavonoids, xanthones, and secoiridoid glycosides (Mahmood et al., 2014). It has laxative, febrifuge, anti-inflammatory, and anti-helminthic properties. *S. chirayita* is also used as a chronic ingredient in anticancer drugs, ayurveda health tonics, antidiabetic preparations, skin creams, hair oils soaps, and even in liver tonics (Shrestha et al., 2015). Herein, we focus on the green fabrication of SnO_2-ZrO_2 and TiO_2@SnO_2-ZrO_2 NCs using *S. chirayita* for first time as capping agent. The physicochemical properties of prepared NCs were investigated via XRD, SEM, DRS, and FTIR techniques. The photocatalytic potential of the prepared nanocomposites was examined against brilliant green and 4-nitrophenol under direct solar light illumination.

ACCEPTED MANUSCRIPT

2 Materials and methods

2.1 Preparation of plant extract

S. chirayita plant was collected from a local area of the Sudhnoti district. It was subsequently washed with distilled water, boiled at 60 °C in 1000 mL water for 3 hours, cooled at room temperature, and then filtered. The filtrate was then stored in an air-tight bottle and subsequently used for the biosynthesis of nanocomposites.

2.2 Synthesis of $Sn(OH)_2$

For the synthesis of $Sn(OH)_2$, 0.98g of $SnCl_2$ salt was taken as a precursor and dissolved in 50 mL water, followed by the addition of 30 mL of plant extract as a stabilizing agent. The solution was heated while being stirred for 45 minutes. Subsequently, NaOH was added to adjust pH which resulted in the preparation of $Sn(OH)_2$ in the basic medium. The solid precipitated nanoparticles were filtered and washed multiple times using distilled water and ethanol to remove any unwanted organic substances. The washed nanoparticles were then dried in an oven at 90 ℃ yielding solid $Sn(OH)_2$ nanoparticles.

2.3 Synthesis of $(ZrOH)_2$

$(ZrOH)_2$ was prepared by dissolving 1.28 g of $ZrCl_2$ in 50 mL water. To this solution, 30 mL of extract was added, acting as a capping and stabilizing agent. It was then heated under stirring for 45 minutes. Following this, NaOH solution was added dropwise to adjust the pH and to promote the precipitation of $(ZrOH)_2$. The solid $Zr(OH)_2$ nanoparticles are collected by filtering the solution. The nanoparticles are washed several times with distilled water and ethanol to remove any unreacted precursors, excess NaOH, and any remaining plant extract or organic by-products. After thorough washing, the nanoparticles were dried in an oven to remove moisture to get dried nanoparticles.

2.4 Synthesis of SnO_2-ZrO_2 NC

The synthesized $Sn(OH)_2$ and $Zr(OH)_2$ (0.5 g each) were hydrolyzed in 100 mL distilled water. To this solution 0.1 M NaOH was added dropwise to attain pH 10. Mixture was heated as well as stirred for 4 hours and then left for aging for 12 hours at room temperature. The resulting precipitates were washed several times using distilled water, oven-dried at 100 °C, and then stored in an air tight glass bottle.

ACCEPTED MANUSCRIPT

2.5 Synthesis of TiO_2@SnO_2- ZrO_2 NC

To synthesize TiO_2@SnO_2- ZrO_2 NC, 1 g of the synthesized SnO_2-ZrO_2 NC was hydrolyzed in 100 mL distilled water to which, the required volume of titanium isopropoxide (for 0.5 % doping) was added that was heated and stirred for 4 hours. The resulting solution was placed under ambient conditions for 12 hours of aging. The precipitates formed were cooled at room temperature, washed several times using distilled water, oven-dried overnight, and finally stored in an air-tight glass bottle.

2.6 Characterization

To evaluate the physicochemical characteristics of prepared samples, various characterization techniques were used. To assess their crystalline properties, X-ray diffraction (XRD) analysis was conducted using the Philips X'Pert model. The crystallite size was calculated by using Debye-Scherrer equation. To examine their microstructure and surface topology, a field emission scanning electron microscope (FE-SEM), specifically the JEOL JSM-5600LV model from Tokyo, Japan, was utilized. The particles size from the SEM images was estimated by using imageJ software. The NOVA Quantachrome version 11.05 was used to study the N_2 adsorption capacity of the prepared samples at a temperature of 77.35 K followed by a degased process at 300 °C. DRS analysis was utilized to examine the light absorbance properties of the samples. Surface functional moieties were analyzed using the Nicolet 560 FTIR spectrometer, covering the range of 4000 to 400 cm^{-1}.

2.7 Photocatalytic activity

Photocatalytic activity of pure and TiO_2 doped SnO_2-ZrO_2 NC was checked against brilliant green and 4-nitrophenol. For each experiment, 20 mg of prepared NCs was added to 50 ml of brilliant green and 4-nitrophenol solutions individually. Prior to sunlight irradiation, the reaction mixture was stirred for 30 min under dark conditions to achieve adsorption-desorption equilibrium. After specific time intervals, the solutions were placed under sunlight, and using a double-beam spectrophotometer, absorbance spectra were recorded to monitor the photocatalytic degradation of brilliant green and 4-nitrophenol.

3 Results and Discussion

The *S. chirayita* extract acted as a green reducing and stabilizing agent during the synthesis. The extract's rich content of bioactive compound i.e. flavonoids, alkaloids, and xanthones that reduced the metal precursors to their metallic or oxide nanoparticle forms. The polyphenols and flavonoids in the extract donate electrons to reduce metal ions and subsequently adsorb onto the nanoparticle surface, forming a stabilizing organic moiety. This functionality controls nanoparticle size and

ACCEPTED MANUSCRIPT

morphology and prevents agglomeration, enabling homogeneous dispersion within the nanocomposite. Further, these compounds cap and stabilize the nanoparticles, preventing agglomeration and enhancing uniformity in size and dispersion. Thus, the extract plays a dual role in both the eco-friendly synthesis and the stabilization of the nanocomposites, aligning with principles of green chemistry. It is expected that the residual phytochemicals on NPs surfaces enhance the generation of ROS during photocatalytic process.

3.1 XRD analysis

XRD was used to determine the average size of crystals as well as the structural composition of the crystalline phase. Figure 1 shows the XRD pattern of pure and TiO_2-doped ZrO_2-SnO_2 NCs. The XRD pattern indicates that the particles have a nanoscale crystallite size, as evidenced by the broad peaks. In XRD spectrum (a), the diffraction bands were observed at 2θ positions of 26.5, 33.86, and 51.8, corresponding to Miller indices (110), (101), and (211), respectively, indicating the tetragonal geometry of nanosized SnO_2 particles. These observations aligned with reference card 01-077-0448. Additionally, a set of Bragg reflections appeared at 2θ positions of 31.9, 34.1, 43.1, 45.1, and 52.1, with corresponding *hkl* values of (012), (111), (022), (121), and (113), respectively, suggesting the rhombohedral geometrical shape of ZrO_2. These findings were consistent with reference card 00-033-1483. In XRD spectrum b, the distinctive Bragg's reflections at corresponding 2θ positions for the TiO_2 doped ZrO_2-SnO_2 NCs showed diffraction peaks with 2θ values of 25.9, 37.86, 54.3, and 62.5, corresponding to Miller indices (101), (004), (211), and (204) respectively. These observations indicated the formation of the anatase phase of titanium dioxide, as per reference card 01-071-1167. The separate sets of diffraction peaks for ZrO_2, SnO_2, and TiO_2 proposed the formation of heterojunction.

ACCEPTED MANUSCRIPT

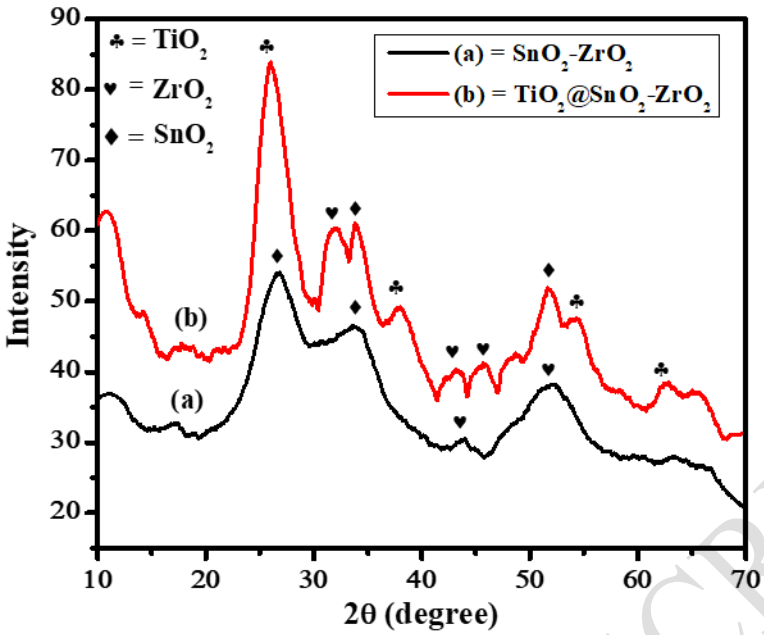

Figure 1: XRD spectra of pure and TiO_2-doped ZrO_2-SnO_2 NCs.

3.2 SEM analysis

The SEM micrographs of the prepared pure and TiO_2 doped SnO_2-ZrO_2 NC at various resolutions shown in Figures 2a and b demonstrate the morphological features of the sample. In the pure SnO_2-ZrO_2 NC (Figure 3a), a predominant large compact structure was observed with multiple smaller agglomerates dispersed across its surface. The image shows a mixed morphological shape of the individual particles, where elongated shapes seem dominant. Moreover, the smaller agglomerates were either nearly spherical, elongated, or polyhedral-shaped, which were unevenly distributed and led to the formation of cavities in the sample. The surface of this structure seemed to be non-porous as well as smooth. Similarly, the SEM image of TiO_2@SnO_2-ZrO_2 NC (figure 3b) displayed a slightly different morphology. Numerous compact structures were obvious where number of cavities had also been decreased. Dispersion of multiple smaller agglomerates over the surface of compact structures was obvious. These agglomerates were multifaceted several of which had distinct boundaries. The size of SnO_2-ZrO_2 ranged between 51.68 to 64.38 nm with an average size of 56.09 nm, whereas the size of TiO_2@SnO_2-ZrO_2 NC lies between 56.85 to 61.68 nm with a mean size of 59.48 nm. The reduction in surface cavities, formation of a more compact structure and increase in average particle size upon TiO_2 doping shows that that the TiO_2 precursors did not form a uniform dopant layer but instead led to partial aggregation and pore blockage.

ACCEPTED MANUSCRIPT

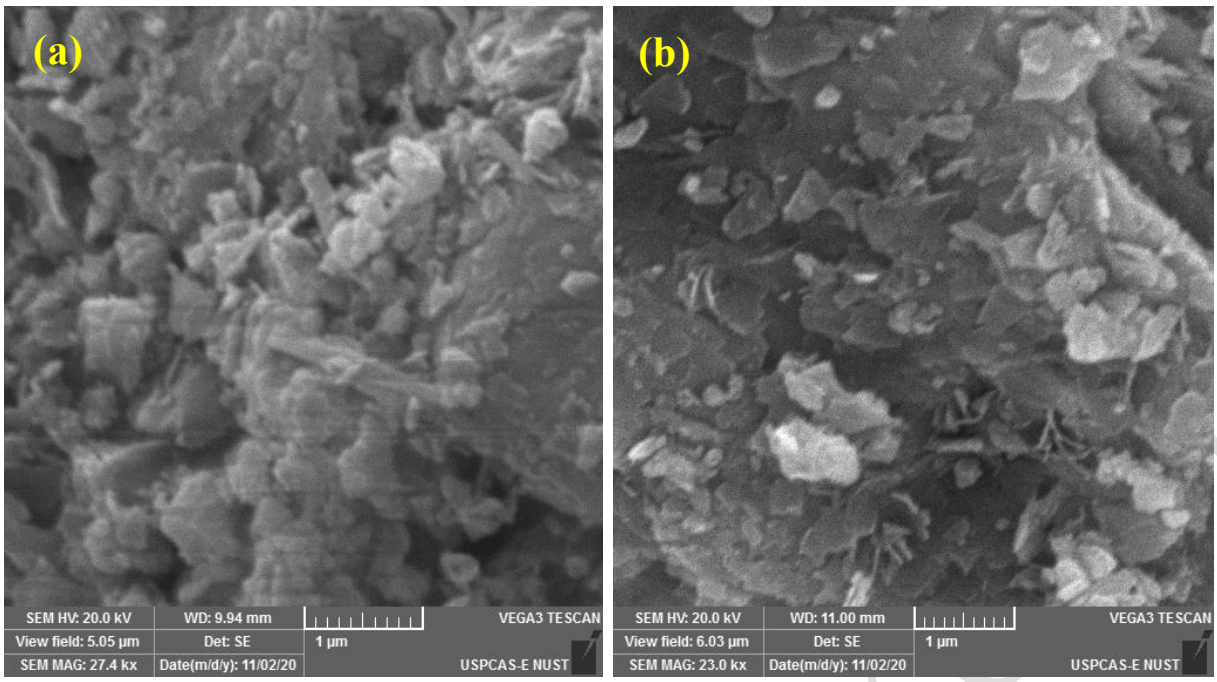

Figure 2: SEM images of pure (a) and TiO_2 doped ZrO_2-SnO_2 NC (b)

3.3 Surface area analysis

The N_2 adsorption experiment was performed to determine the surface area of the synthesized pure and TiO_2-doped SnO_2-ZrO_2 NCs, where the adsorption data was analyzed using the BET equation as shown in Figure 3. The results show that the adsorption was maximum at zero relative pressure and was found to decrease with increasing relative pressure. The surface area was found to be 96.04 and 29.75 m^2/g for SnO_2-ZrO_2 and TiO_2-doped SnO_2-ZrO_2 NC, respectively. Moreover, the surface area of the samples was seen to decrease after doping the SnO_2-ZrO_2 NC with TiO_2. This decrease might be attributed to the surface coverage of the SnO_2-ZrO_2 NC, which preferentially occupies the surface sites (pores), which can reduce the accessibility of the surface area for the adsorbent to adsorb. The insertion of TiO_2 also induced structural changes in the SnO_2-ZrO_2 matrix, which may affect the growth and crystallinity, leading to the formation of larger crystallites that can reduce the surface area-to-volume ratio (Lee et al., 2004).

ACCEPTED MANUSCRIPT

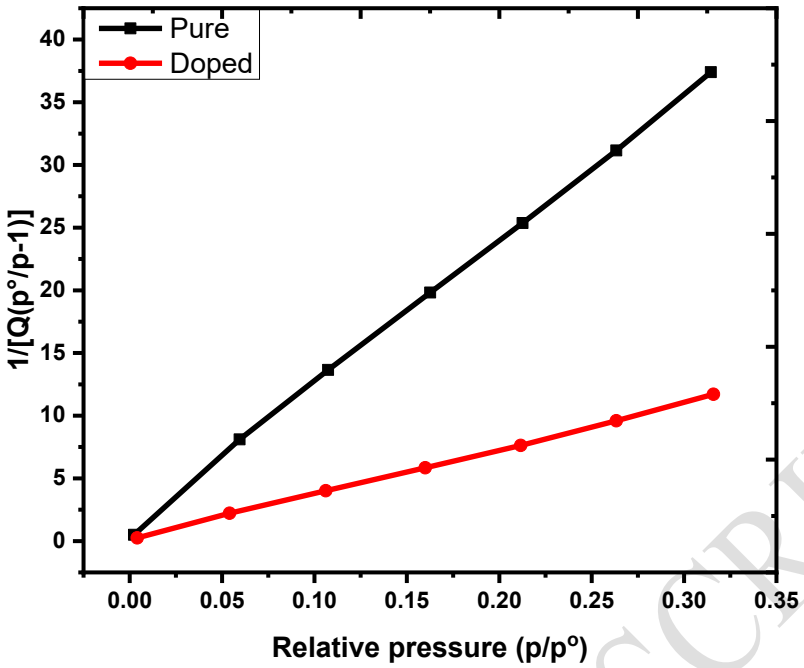

Figure 3: BET plots of pure and TiO_2 doped SnO_2-ZrO_2 NC

3.4 DRS analysis

The DRS spectra of pure and TiO_2-doped SnO_2-ZrO_2 NCs were recorded within the range of 250-800 nm as depicted in Figure 4. DRS spectra indicated the presence of transmittance edge at 300.78 and 294.14 nm. This slight shift of the absorption band to a longer wavelength after doping of TiO_2 might be due to the quantum size effect and the creation of oxygen vacancies (Kaningini et al., 2022). The Tauc plot method was applied to calculate the direct band gap energy of both samples, which are found to be 3.41 eV and 3.47 eV. The TiO_2 doping leading to an increase in band gap from 3.41 eV to 3.47 eV is a key indicator of a potential phase mismatch. Instead of creating beneficial narrowness electronic states within the band gap, the incorporation of TiO_2 may have formed a separate, poorly integrated phase or induced lattice strain. This can create energy barriers at the interfaces between Sn-Zr oxide and TiO_2, hindering the smooth transfer of photogenerated charge carriers i.e. electrons and holes and promoting their recombination before they can participate in surface reactions (Azam et al., 2012).

ACCEPTED MANUSCRIPT

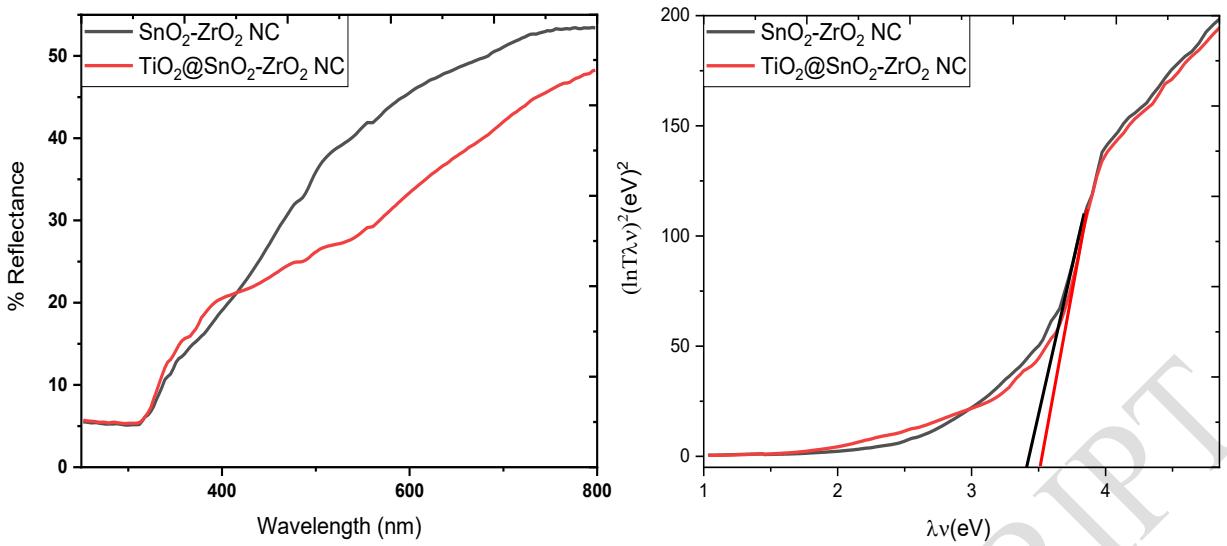

Figure 4: DRS spectra and the Tauc plot for the direct band of pure and TiO_2-doped ZrO_2-SnO_2 NCs.

3.5 FTIR analysis

FTIR spectra of prepared pure and TiO_2-doped ZrO_2-SnO_2 NCs are depicted in the figure 5. A broad band appeared in the range of 3500-3000 cm^{-1} corresponding to stretching vibrations of the O–H group present in water molecules and surface metal hydroxide bonds (Aghabeygi et al., 2018). The band obtained at 2335 cm^{-1} was due to surface-absorbed carbon dioxide molecules during the synthesis (Chikkanna et al., 2019). The peak observed at 1628 cm^{-1} in spectra of the pure composite was ascribed to bending vibrations of OH while the band at 895 cm^{-1} was accredited to the Sn-O-Zr bond (Qiu et al., 2015). Moreover, the absorption band obtained at 626 cm^{-1} was a characteristic band of tin oxide (Maeda et al., 1995). The band observed at 532 cm^{-1} corresponding to the terminal oxygen vibration of SnO_2 material while in the titanium dioxide-doped composite, the band obtained at 1622 cm^{-1} indicated the bending vibration of the Ti–OH bond (Zhao et al., 2018). The bands detected at 1346 cm^{-1} and 586 cm^{-1} were attributed to the Zr-O bond (Singh et al., 2015).

ACCEPTED MANUSCRIPT

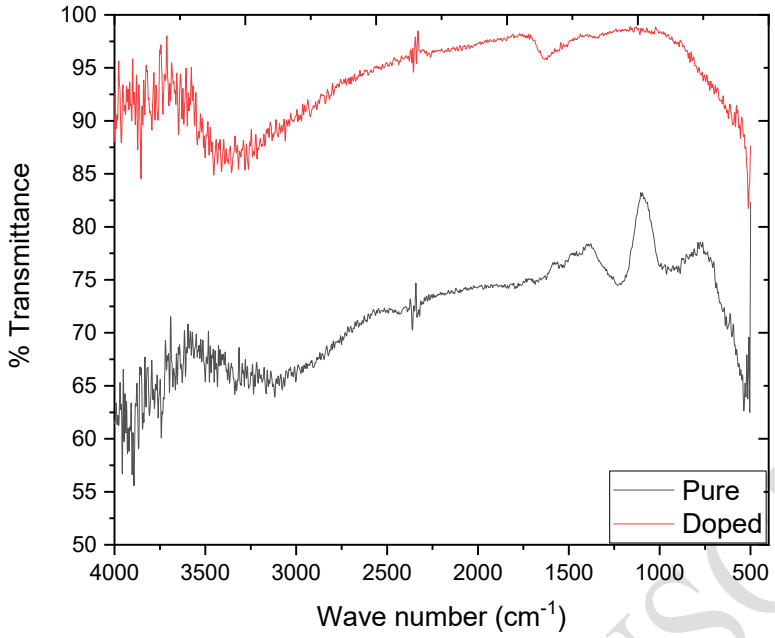

Figure 5: FTIR spectra of pure and TiO_2-doped ZrO_2-SnO_2 NC.

3.6 Photocatalytic activity

Pure and TiO_2-doped SnO_2-ZrO_2 NCs were used to photocatalytically degrade synthetic organic pollutants i.e., brilliant green and 4-nitrophenol. The prepared photocatalysts (20 mg) were added to 50 mL of brilliant green and 4-nitrophenol solutions separately, and then aluminum foil was used to cover the beakers. To attain adsorption-desorption equilibrium, the solution was initially stirred using a magnetic stirrer for 30 minutes in the dark, after which, it was exposed to sunlight between 11 am to 2 pm (18 June, 2024). The color of the solution faded with the passage of time suggesting the degradation of the functional moiety responsible for light absorption. After a specific time interval, the progress of the reaction was monitored via a spectrophotometer.

3.6.1 Degradation Profile

The photo-induced degradation of both pollutants was constantly examined by a double beam spectrophotometer and the decrease in the absorbance maxima was noted as function of time interval as shown in Figure 6 (a and b). A gradual decrease in the absorbance maxima was observed, suggesting the degradation of the organic pollutants. The results reveal a sharp decrease in the absorbance maxima of the 4-nitrophenol as compared to brilliant green with respect to irradiation time. This shows the high degradation potential of the prepared nanocatalysts against 4-nitrophenol as compared to brilliant green.

ACCEPTED MANUSCRIPT

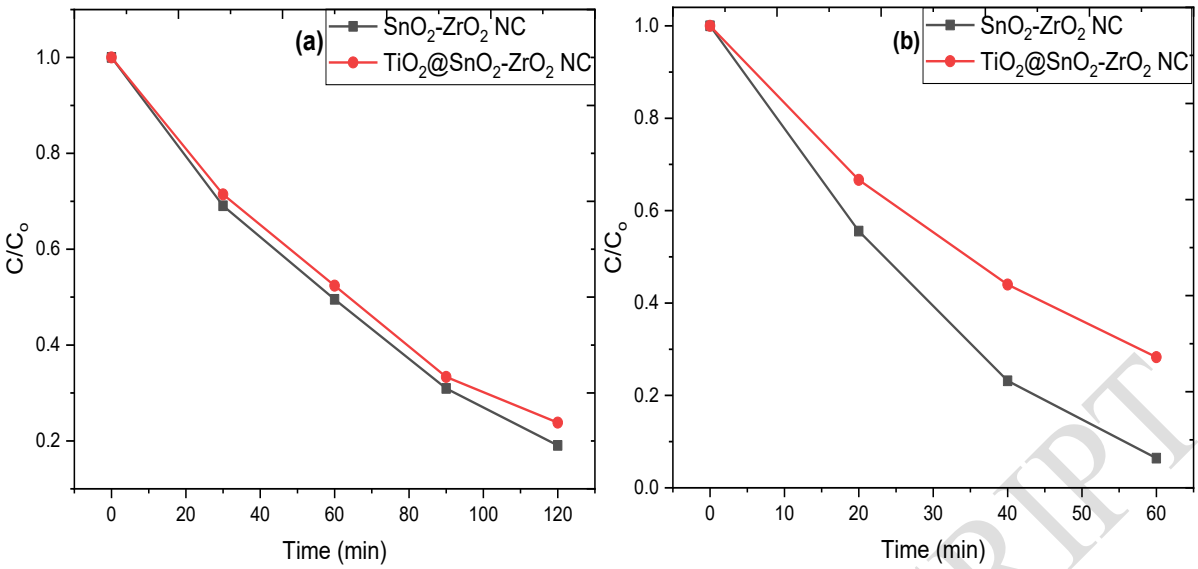

Figure 6: Degradation profile of brilliant green (a) and 4-nitrophenol (b).

3.6.2 Percentage degradation

The percentage degradation of both pollutants (Figure 7) was determined by using equation 1, where C_o is the initial concentration while C_e represents the concentration of pollutants at a specific time. (Bibi et al., 2020; Shoukat et al., 2019) The results show that 80.9% and 77% of the brilliant green were degraded by SnO_2-ZrO_2 NC and TiO_2@ SnO_2-ZrO_2 NC in 120 min, respectively. Likewise, 93.57 and 71.70 % of the 4-nitrophenol were degraded in 60 min in the presence of SnO_2-ZrO_2 NC and TiO_2@SnO_2-ZrO_2 NC, respectively. It is evident from the results that the synthesized nanocatalysts show high efficacy against 4-nitrophenol as compared to the brilliant green. The study demonstrates the potential of SnO_2-ZrO_2 NC and TiO_2@SnO_2-ZrO_2 NC as effective catalysts for the degradation of organic pollutants.

$$\%\ degradation = \frac{co-ce}{co} \times 100 \qquad (1)$$

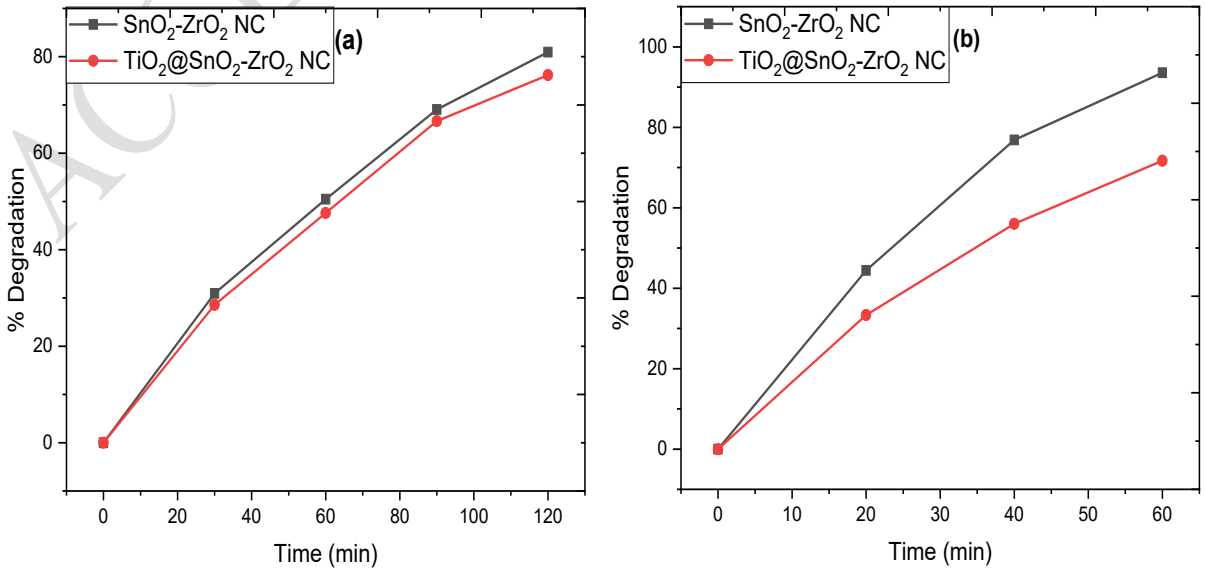

ACCEPTED MANUSCRIPT

Figure 7: Percentage degradation profile of brilliant green (a) and 4-nitrophenol (b).

3.6.3 Kinetic study

The kinetic study of the photodegradation reaction of both pollutants was performed by applying equation 2 and the obtained plots are shown in Figure 8. The degradation rate constant for SnO_2-ZrO_2 NC was found to be 1.373 x 10^{-2} min^{-1} while for TiO_2@ SnO_2-ZrO_2NC, it was 1.211 x 10^{-2} min^{-1} against brilliant green. In the case of 4-nitrophenol, the 4.56 x 10^{-1} min^{-1} and 2.78 x 10^{-4} min^{-1} rate constants were determined for SnO_2-ZrO_2 NC and TiO_2@ SnO_2-ZrO_2NC. In the case of both pollutants, the slow degradation rate found for the doped sample suggests the low photocatalytic potential of the catalyst. As it was also assumed from the surface area and band gap analysis, the TiO_2@SnO_2-ZrO_2 NC would have low photocatalytic potential.

$$ln\frac{C}{Co} = -kt \qquad (2)$$

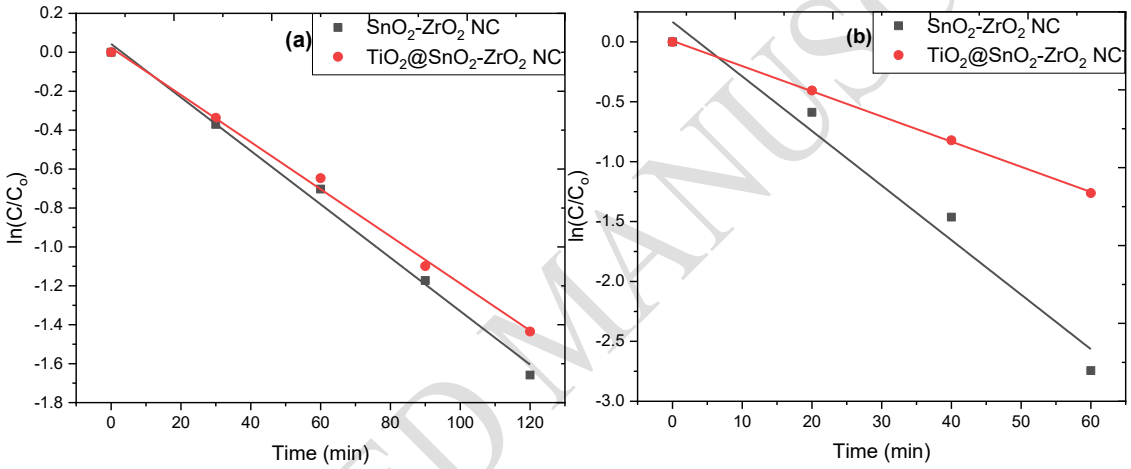

Figure 8: Degradation rate constant; (a) brilliant green, b) 4-nitrophenol.

3.6.4 Photocatalytic reaction mechanism

When the nanocomposite is exposed to solar or UV light, photons with energy greater than the band gap of the catalyst are absorbed, which leads to the generation of electron-hole pairs in the valance band (VB) of all the three counterparts i.e., SnO_2, TiO_2, and ZrO_2 of the nanocomposite as shown in Figure 9. Once generated, the photoexcited electrons (e^-) migrate from the VB to the conduction band (CB), leaving behind positively charged holes (h^+) in the VB. The excited electrons gather in the CB of TiO_2 whereas the generated h^+ are shifted to VB of ZrO_2. The electrons in the CB of TiO_2 and the holes in the VB are highly reactive and participate in redox reactions with adsorbed species on the catalyst surface. The holes can oxidize organic dye molecules (Dye) adsorbed on the surface, leading to the formation of radical cations ($Dye^{+\bullet}$). Meanwhile, the electrons in the CB can reduce oxygen molecules (O_2) to form superoxide radicals ($\bullet O^{2-}$). The highly reactive radical cations and superoxide radicals generated on the catalyst surface then attack the organic dye molecules adsorbed onto the surface, breaking down their chemical structure into smaller, less harmful molecules, such as carbon

ACCEPTED MANUSCRIPT

dioxide (CO_2) and water (H_2O). To maintain the photocatalytic activity, minimizing the recombination of electron-hole pairs is essential. Dopants like zirconium dioxide and tin dioxide in the nanocomposite can help to reduce the recombination rate by trapping the photoexcited electrons and holes, thereby prolonging their lifetime.

The variation in the photocatalytic activity of the catalysts might be due to the molecular structure and reactivity of both pollutants. The 4-nitrophenol has a simpler structure with a nitro group attached to the phenol, whereas the brilliant green has a more complex molecular structure with multiple substituted benzene rings. The structural complexity of the pollutants makes them more resistant to degradation. Moreover, the electron-removing nature of the nitro group makes 4-nitrophenol more susceptible to degradation by the reaction of hydroxyl radicals (•OH).

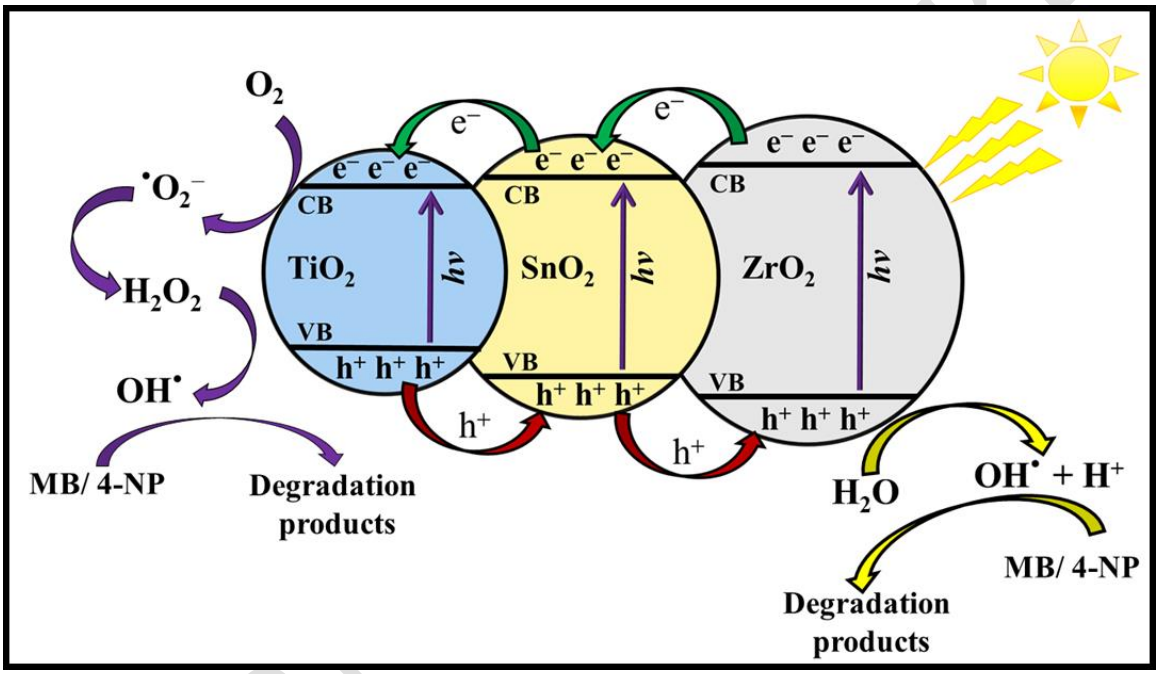

Figure 9: Illustration of photodegradation mechanism of organic pollutants in the presence of pure and TiO_2-doped ZrO_2-SnO_2 NCs.

3.6.5 Comparative analysis

Table 1 shows the comparative analysis of the photocatalytic performance of our catalyst with values reported in the literature. The metrics presented are the time of reaction and dose of the catalysts required to obtain maximum degradation of the pollutant. Under these standardized criteria, our prepared catalyst demonstrates significantly higher activity, achieving greater degradation in shorter times than most reported catalysts. This enhanced performance is reflected in both the shorter times and low dose to reach to higher degradation percentages.

ACCEPTED MANUSCRIPT

Table 1: comparative analysis of the-photocatalytic efficacy of the current catalyst with reported data

Catalysts	Dye	Dose (mg/L)	Time (min)	% degradation	References
$Sr_{0.4}Ba_{0.2}Fe_2O_4$	Atrazine	10	75	86.48	(Yasar et al., 2025)
CuO-NiO-NC	Rhodamine 6G	20	60	80.09	(Lone et al., 2025)
GO-CeO_2	Methylene blue		120	100	(Fauzia et al., 2024)
ZnO-NPs	Methyl orange	75	250	87	(Mousa et al., 2024)
SnO_2-ZrO_2 NC	Brilliant green	20	120	80.9	Current study
SnO_2-ZrO_2 NC	4-nitrophenol	20	60	93.57	Current study

4 Conclusions

The ZrO_2-SnO_2 and TiO_2-doped ZrO_2-SnO_2 NCs were successfully synthesized using an eco-friendly method employing *S. chirayita* extract as a capping and stabilizing agent. XRD analysis demonstrates that ZrO_2-SnO_2 and TiO_2-doped ZrO_2-SnO_2 NCs nanocomposites possess crystalline structures with nanoscale crystallite sizes. DRS analysis showed an increase in band gap energy from 3.42 eV to 3.37 eV which can be attributed to quantum confinement and structural variation. The SEM analysis shows that agglomeration of nanoparticles in both composites with an average size of 56.09 nm for SnO_2-ZrO_2 and 59.48 nm TiO_2-doped ZrO_2-SnO_2 NCs respectively. Moreover, BET analysis was carried out for surface area determination which was found to be 96.04 m^2/g for SnO_2-ZrO_2 and 29.75 m^2/g for TiO_2-doped SnO_2-ZrO_2 nanocomposites, respectively. The green synthesized SnO_2-ZrO_2 demonstrated higher photocatalytic potential for degradation of brilliant green and 4-nitrophenol as compared to doped sample. This boosted activity of SnO_2-ZrO_2 NC was mainly due to lower band gap energy and higher surface area which cause efficient generation of electron-hole pairs as well as faster adsorption owing to its enhanced surface area. This work offers a green and non –toxic approach utilizing plant extract for the synthesis of nanocomposites. This work can be extended by selectively doping the SnO_2-ZrO_2 NC with metals to lower its band gap to further improve its photocatalytic performance. Similarly, other plants' ectract can also be used to study their influence on morphological variation leading to a variation in photocatalytic potential.

ACCEPTED MANUSCRIPT

Acknowledgments: The authors extend their appreciation to Taif University, Saudi Arabia, for supporting this work through project number (TU-DSPP-2024-158).

References

Aghabeygi, S., & Khademi-Shamami, M. (2018). ZnO/ZrO2 nanocomposite: Sonosynthesis, characterization and its application for wastewater treatment. *Ultrasonics Sonochemistry*, *41*(June 2017), 458–465. doi: 10.1016/j.ultsonch.2017.09.020

Anwer, H., Mahmood, A., Lee, J., Kim, K., Park, J., & Yip, A. C. K. (2019). *Photocatalysts for degradation of dyes in industrial effluents : Opportunities and challenges*. *12*(5), 955–972.

Azam, A., Ahmed, A. S., Habib, S. S., & Naqvi, A. H. (2012). Effect of Mn doping on the structural and optical properties of SnO 2 nanoparticles. *Journal of Alloys and Compounds*, *523*, 83–87. doi: 10.1016/j.jallcom.2012.01.072

Bibi, N., Haq, S., Rehman, W., Waseem, M., Rehman, M. U., Shah, A., Khan, B., & Rasheed, P. (2020). Low temperature fabrication of SnO2, ZnO and Zn2SnO4 nanostructures for the degradation of Rhodamine 6G: characterization. *Biointerface Research in Applied Chemistry*, *10*(4), 5895–5900.

Bona, A. Della, Pecho, O. E., & Alessandretti, R. (2015). Zirconia as a dental biomaterial. *Materials*, *8*(8), 4978–4991. doi: 10.3390/ma8084978

Chikkanna, M. M., Neelagund, S. E., & Rajashekarappa, K. K. (2019). Green synthesis of Zinc oxide nanoparticles (ZnO NPs) and their biological activity. *SN Applied Sciences*, *1*(1), 1–10. doi: 10.1007/s42452-018-0095-7

Chowdhury, M., Sultana, S., Armin, M., Hossain, M., Dey, S., & Naznin, H. (2019). *Review on various types of pollution problem in textile dyeing & printing industries of Bangladesh and recommandation for mitigation*. *5*(4), 220–226. doi: 10.15406/jteft.2019.05.00205

Fauzia, Khan, M. A., Chaman, M., & Azam, A. (2024). Antibacterial and sunlight-driven photocatalytic activity of graphene oxide conjugated CeO2 nanoparticles. *Scientific Reports*, *14*(1), 1–17. doi: 10.1038/s41598-024-54905-0

Haq, S., Afsar, H., Ali, M. Ben, Almalki, M., Albogami, B., & Hedfi, A. (2021). Green Synthesis and Characterization of a ZnO–ZrO2 Heterojunction for Environmental and Biological Applications. *Crystals*, *11*, 1–12.

Haq, S., Afsar, H., Din, I. U., Ahmad, P., Khandaker, M. U., Osman, H., Alamri, S., Shahzad, M. I., Shahzad, N., Rehman, W., & Waseem, M. (2021). Enhanced photocatalytic activity of ficus elastica mediated zinc oxide-zirconium dioxide nanocatalyst at elevated calcination temperature: Physicochemical study. *Catalysts*, *11*(12), 1–15. doi: 10.3390/catal11121481

ACCEPTED MANUSCRIPT

Haq, S., Rehman, W., & Rehman, M. (2020). Modeling, Thermodynamic Study and Sorption Mechanism of Cadmium Ions onto Isopropyl Alcohol Mediated Tin Dioxide Nanoparticles. *Journal of Inorganic and Organometallic Polymers and Materials*, *30*(4), 1197–1205. doi: 10.1007/s10904-019-01256-3

Haq, S., Rehman, W., & Waseem, M. (2018). Adsorption Efficiency of Anatase TiO2 Nanoparticles Against Cadmium Ions. *Journal of Inorganic and Organometallic Polymers and Materials*, *29*(3), 651–658. doi: 10.1007/s10904-018-1038-x

Haq, S., Rehman, W., Waseem, M., Meynen, V., Awan, S. U., Khan, A. R., Hussain, S., Zain-ul-Abdin, Din, S. U., Hafeez, M., & Iqbal, N. (2021). Effect of Annealing Temperature on Structural Phase Transformations and Band Gap Reduction for Photocatalytic Activity of Mesopores TiO2 Nanocatalysts. *Journal of Inorganic and Organometallic Polymers and Materials*, *31*(3), 1312–1322. doi: 10.1007/s10904-020-01810-4

Haq, S., Sarfraz, A., Menaa, F., Shahzad, N., Din, S. U., Almukhlifi, H. A., Alshareef, S. A., Al Essa, E. M., & Shahzad, M. I. (2022). Green Synthesis of NiO-SnO2 Nanocomposite and Effect of Calcination Temperature on Its Physicochemical Properties: Impact on the Photocatalytic Degradation of Methyl Orange. *Molecules*, *27*(23), 1–19. doi: 10.3390/molecules27238420

Haq, S., Shoukat, S., Rehman, W., Waseem, M., & Shah, A. (2020). Green fabrication and physicochemical investigations of zinc-cobalt oxide nanocomposite for wastewater treatment. *Journal of Molecular Liquids*, *318*, 114260. doi: 10.1016/j.molliq.2020.114260

Kaningini, A. G., Azizi, S., Sintwa, N., Mokalane, K., Mohale, K. C., Mudau, F. N., & Maaza, M. (2022). Effect of Optimized Precursor Concentration, Temperature, and Doping on Optical Properties of ZnO Nanoparticles Synthesized via a Green Route Using Bush Tea (Athrixia phylicoides DC.) Leaf Extracts. *ACS Omega*, *7*(36), 31658–31666. doi: 10.1021/acsomega.2c00530

Karak, N. (2019). Fundamentals of Nanomaterials and Polymer Nanocomposites. In Nanomaterials and Polymer Nanocomposites. Elsevier Inc. doi: 10.1016/B978-0-12-814615-6.00001-1

Konecoglu, G., Safak, T., Kalpakli, Y., & Akgun, M. (2015). Photocatalytic degradation of textile dye CI Basic Yellow 28 wastewater by Degussa P25 based TiO_2. *Advances in Environmental Research*, *4*(1), 25–38. doi: 10.12989/aer.2015.4.1.025

Lee, Y.-J., Uchiyama, Y., & Radovic, L. R. (2004). Effects of boron doping in low-and high-surface-area carbon powders. *Carbon*, *42*(11), 2233–2244.

Lellis, B., Fávaro-polonio, C. Z., Pamphile, J. A., & Polonio, J. C. (2019). *Effects of textile dyes on health and the environment and bioremediation potential of living organisms*. doi: 10.1016/j.biori.2019.09.001

Li, P., Guo, M., Wang, Q., Li, Z., Wang, C., Chen, N., Wang, C. C., Wan, C., & Chen, S. (2019).

ACCEPTED MANUSCRIPT

Controllable synthesis of cerium zirconium oxide nanocomposites and their application for photocatalytic degradation of sulfonamides. *Applied Catalysis B: Environmental*, *259*(August), 118107. doi: 10.1016/j.apcatb.2019.118107

Lone, A. L., Rehman, S. U., Haq, S., Alkhuriji, A. F., Al-Malahi, N. M., Razzokov, J., Shujaat, S., & Samad, A. (2025). Fabrication and structural analysis of CuO-NiO and MWCNTs@CuO-NiO hybrid nanostructures: versatile materials for environmental and biomedical remediation. *RSC Advances*, *15*(28), 22311–22321. doi: 10.1039/d5ra02443a

Maeda, S., & Armes, S. P. (1995). Preparation and Characterization of Polypyrrole-Tin(IV) Oxide Nanocomposite Colloids. *Chemistry of Materials*, *7*(1), 171–178. doi: 10.1021/cm00049a026

Mahmood, S., Hussain, S., Tabassum, S., Malik, F., & Riaz, H. (2014). Comparative phytochemical, hepatoprotective and antioxidant activities of various samples of Swertia Chirayita collected from various cities of Pakistan. *Pakistan Journal of Pharmaceutical Sciences*, *27*(6), 1975–1983.

Malik, A., Akhtar, R., & Grohmann, E. (2014). Environmental deterioration and human health: Natural and anthropogenic determinants. *Environmental Deterioration and Human Health: Natural and Anthropogenic Determinants*, 1–421. doi: 10.1007/978-94-007-7890-0

Mousa, S. A., Wissa, D. A., Hassan, H. H., Ebnalwaled, A. A., & Khairy, S. A. (2024). Enhanced photocatalytic activity of green synthesized zinc oxide nanoparticles using low-cost plant extracts. *Scientific Reports*, *14*(1), 1–18. doi: 10.1038/s41598-024-66975-1

Pouretedal, H. R., Tofangsazi, Z., & Keshavarz, M. H. (2012). *nanoparticles*. *513*, 359–364. doi: 10.1016/j.jallcom.2011.10.049

Qiu, H., Liang, C., Zhang, X., Chen, M., Zhao, Y., Tao, T., Xu, Z., & Liu, G. (2015). *Fabrication of a Biomass-based Hydrous Zirconium Oxide Nanocomposite for Preferable Phosphate Removal and Recovery Fabrication of a Biomass-based Hydrous Zirconium Oxide Nanocomposite for Preferable Phosphate Removal and Recovery*. doi: 10.1021/acsami.5b06098

Roushan, K., Fereydouni, S., & Bahrami, L. (2016). Enhanced photocatalytic activity of nanocomposites of TiO 2 doped with Zr , Y or Ce polyoxometalates for degradation of methyl orange dye Roushan Khoshnavazi , Shler Fereydouni and Leila Bahrami. *Water Science and Technology*, *73*(7), 1746–1755. doi: 10.2166/wst.2016.008

Ruan, W., Hu, J., Qi, J., Hou, Y., Zhou, C., & Wei, X. (2019). Removal Of Dyes From Wastewater By Nanomaterials : A Review. *Advanced Materials Letters*, *10*(1), 9–20. doi: 10.5185/amlett.2019.2148

Sadat, M., & Sahar, M. (2016). Simple salt-assisted combustion synthesis of Nd 2 Sn 2 O 7 – SnO 2 nanocomposites with different amino acids as fuel : an efficient photocatalyst for the degradation of methyl orange dye. *Journal of Materials Science: Materials in Electronics*, 2–10. doi:

ACCEPTED MANUSCRIPT

10.1007/s10854-016-5306-7

Salama, A., Mohamed, A., Aboamera, N. M., Osman, T. A., & Khattab, A. (2018). Photocatalytic degradation of organic dyes using composite nanofibers under UV irradiation. *Applied Nanoscience (Switzerland)*, *8*(1–2), 155–161. doi: 10.1007/s13204-018-0660-9

Shoukat, S., Rehman, W., Haq, S., Waseem, M., & Shah, A. (2019). Synthesis and characterization of zinc stannate nanostructures for the adsorption of chromium (VI) ions and photo-degradation of rhodamine 6G. *Materials Research Express*, *6*(11), 115052. doi: 10.1088/2053-1591/ab473c

Shrestha, P., Bista, M., Sharma, P., Shrestha, S., Lamichhane, B., Adhikari, S., Pandey, B. R., & Shrestha, B. G. (2015). Phytochemical screening, antimicrobial activity and cytotoxicity of Nepalese medicinal plants Swertia chirayita and Dendrobium amoenum. *Nepal Journal of Biotechnology*, *3*(1), 48–57. doi: 10.3126/njb.v3i1.14231

Singh, B. R., Shoeb, M., Khan, W., & Naqvi, A. H. (2015). AC SC. In Journal of Alloys and Compounds. Elsevier Ltd. doi: 10.1016/j.jallcom.2015.05.231

State, A. (2011). *Industrial Effluents and Their Impact on Water Quality of*. *1*(1), 75–86.

Wibowo, Y. G., Anwar, D., Safitri, H., Surya, I., Sudibyo, S., Yuliansyah, A. T., & Murti Petrus, H. T. B. (2025). Functionalized magnetite-biochar with live and dead bacteria for adsorption-biosorption of highly toxic metals: Cd, Hg, and Pb. *Next Materials*, *6*(January), 100487. doi: 10.1016/j.nxmate.2025.100487

Wibowo, Y. G., Lululangin, B. R. G., Safitri, H., Rohman, A., Priyanto, S., Syarifuddin, H., Maryani, A. T., Yuliansyah, A. T., Kurniawan, A., & Nur'ani, H. (2023). Rapid and highly efficient adsorption of dye and heavy metal on low-cost adsorbent derived from human feces and chlorella vulgaris. *Environmental Nanotechnology, Monitoring & Management*, *20*, 100905.

Wibowo, Y. G., Safitri, H., Kusumawati, Aini, W. D., Farantino, R., Ginting, S. B., Rinovian, A., Kurniawan, S. B., Khairurrijal, K., Taher, T., Kusumaningrum, W. B., Sudibyo, S., Yuliansyah, A. T., & Petrus, H. T. B. M. (2025). Biochar MMT ZnAl LDH composite materials derived from solid waste for heavy metal removal in artificial acid mine drainage. *Scientific Reports*, *15*(1), 1–17. doi: 10.1038/s41598-025-96987-4

Yasar, M., Kadhem, A. A., Alzahrani, F. M., Fatima, K., Kalandarov, A., Liliya, A., Mehdi, M. M., Alzahrani, K. J., & Madni, M. (2025). Influence of Nickel Doping on the Photocatalytic Activity of Strontium Barium Ferrite for the Degradation of Atrazine under Photon-Fenton System. *Catalysis Letters*, *155*(5). doi: 10.1007/s10562-025-05009-5

Zhao, J., Ge, S., Pan, D., Shao, Q., Lin, J., Wang, Z., Hu, Z., Wu, T., & Guo, Z. (2018). Solvothermal synthesis, characterization and photocatalytic property of zirconium dioxide doped titanium dioxide spinous hollow microspheres with sunflower pollen as bio-templates. *Journal of Colloid and Interface Science*, *529*, 111–121. doi: 10.1016/j.jcis.2018.05.091

ACCEPTED MANUSCRIPT

ACCEPTED MANUSCRIPT